Particle Orbits in General Relativity: from Planetary Solar System to Black Hole Environment

Kirill Vankov

Particle Orbits in General Relativity: from Planetary Solar System to Black Hole Environment

Kirill Vankov
kirill.vankov@gmail.com

August 3, 2017

Abstract

In this work, we present results of our study of particle dynamics in General Relativity in the whole range of a gravitational field strength. The study is focused on the methodologies of problem formulations, predictions of principally observable characteristics of orbits, and criteria of comparison with Classical (Newtonian) Physics. Methods of both numerical integration and analytic (elliptic functions) theory are used in their comparison. Among new results are the exact solutions of angular and time dependent problems. Complete classification of different orbit types is deduced. The main reputed references related to the work are given with comments.

Contents

1 Historical Notes in Brief

The problem of the test particle motion in the gravitational field due to a central force was originally posed by Einstein in 1915 [1] to finally brush up General Relativity (GR) as the theory of gravitational field. He was excited to find out that the equation of motion derived from his field equations approximately explains the value of "Mercury's anomalous perihelion advance" at that time speculated by astronomers. The Mercury test is crucial for GR theory verification. Einstein's derivation of the effect was based on some assumptions and approximations, among which, weak field conditions in the scheme of "a perturbation of the classical equation" [2, 3].

The responding publications of different authors on the subject have actually been repetitions of Einstein's methodology of particle dynamics, to the exclusion of work by Hagihara [4], (1931). He published his monograph about the application of the theory of elliptic functions for deriving exact analytic solution of Einstein's problem, in particular, concerning the Mercury's perihelion anomaly. Obviously, technical level of computations in early thirties was too low to realize the method in practice so, the results were of qualitative interest. Historically, efforts were focused on the long-standing problem of "the Mercury's anomalous motion" and similar problems under weak-field conditions. The predicted GR effects must be seen as very small deviations from the classical theory.

Later on, Chandrasekhar [5] (1983) studied the problem analytically in terms of elliptic function solution in relationship with the GR Black Hole (BH) concept. However, he modified original Einstein's equation in order to obtain a simplified numerical solution in terms of classical geometrical parameter ("an effective eccentricity") in combination with effective physical parameters. Consequently, the solution deviated from the exact one, the difference having not being evaluated, that made difficult to reveal GR non-classical aspects of space-time curvature. The GR Mercury problem was not studied.

Recently, Kraniotis and Whitehouse [6] (2003) used the theory of elliptic functions to obtain the exact solution in order to reproduce Einstein's GR prediction of Mercury's anomaly. Even before this publication, there was a wide belief among Physics community that the above Einstein's problem had been fully studied with no questions left. In reality, in their work for the first time the exact angular solution to the Mercury's problem was realized, in contrast to previously pub-

lished approximate solutions. However, such issues as an extension of the method to general conditions of arbitrary field strength, the time-dependent problems, and the comparison of GR versus Newtonian predictions were not studied.

Over time, the treatment of the problem has changed after finding the Schwarzschild metric being an exact solution to Einstein's field equation (EFE). Nowadays, the original Einstein's equation of particle motion is considered valid in the whole range of field strength. If so, it allows studying New Physics phenomena with greater GR effects, for example, in hypothetical super-massive Black Holes.

In this work, we study methodologies of the problem formulation in the whole range of field strength. At the same time, the attention is paid to practical realization of exact (numerical and analytic) solutions and demonstrations of GR effects such as in the GR Mercury's orbit and Black Holes. An unambiguous formulation of initial conditions is shown to be crucial. Our goal is to ensure that an adequate physical interpretation of the results is rigorously substantiated in the GR academic framework. Essential methodological and computational novelties, and new results of calculations are claimed.

Among new results are the exact solutions of angular and time dependent problems. The main reputed references related to the work are given with comments. A detailed review of Mercury's observations and their treatments can be found in [7].

2 GR particle dynamics

2.1 Formulation of the physical problem

One of the goals of this work is a scientific justification of the GR verifiable predictions of particle motion in the Schwarzschild field. We study the exact solutions to the traditional problem of Einstein's angular perihelion advance in terms of orbiting radius function $r(\theta)$ as well as the time dependent problem $r(t)$, which was not paid attention in literature. Due to an extreme smallness of the GR effect, a rigorous formulation of the problem is important to provide a high precision of its solutions in parts of methodology, calculations, and comparisons of the results with Newtonian Physics.

Given the GR equation and prior to attempt to solve it, one has to unambiguously fix the initial conditions and choose a minimal number

of independent physical parameters, which determine a unique solution in connection with observables. Otherwise, the solution could be spoiled. In the next step, it should be decided how the solution could be correctly compared with the corresponding solution in classical mechanics.

2.2 The GR equation of particle dynamics

The equation of GR particle dynamics in polar coordinates was originally presented by Einstein in [1] more than hundred years ago

$$\left(\frac{\mathrm{d}x}{\mathrm{d}\theta}\right)^2 = \frac{2\,A}{B^2} + \frac{\alpha}{B^2}x - x^2 + \alpha\,x^3\,, \tag{1}$$

where $x = 1/r$ is the inverted radius; A and B are the total energy and the angular momentum, correspondingly; $\alpha = 2\,r_g = 2\,G\,M/c^2$ is the Schwarzschild radius (r_g is the gravitational radius). Here, the mass of gravitational field source M is however greater than the mass of the test particle, $M \gg m$. This is an unfortunate restriction because otherwise the equation cannot be strictly derived from the EFE [8]. As a consequence, one cannot introduce the center of mass to account for the finite mass of orbiting body or several interacting bodies, as in the case of the planet Mercury.

In the contemporary presentation, unlike in [1], the equation explicitly includes the term of particle proper mass/energy. Classical components of the total energy are summed up quadratically in a way apparently showing their smallness in comparison with the proper mass term. The cubic GR term makes the equation principally different from the corresponding classical equation. Under the weak field conditions, the term of potential energy is as small as $r_g/r_0 \ll 1$ given in the dimensionless form, where r_0 is the distance of the test particle from the source, and the speed of light $c = 1$.

With the field strength, the GR effect can drastically rise. Say, for (r_g/r_0) in the range 0.001–0.1, the test particle can reach the speed close to the speed of light. Under certain extreme conditions, it could be higher and interpreted in terms of superluminal motion.

2.3 Lagrangian solution

The way of the equation derivation may affect the interpretation of its solution. Nowadays, there are several approaches to how to derive the

equation in the contemporary presentation. Kraniotis and Whitehouse [6] review on how it goes from the EFE with the use of Christoffel symbols under conditions of spherical symmetry. Alternatively, it is derived from the Schwarzschild metric [9, 10].

A more quick way is based on the Hamiltonian Action Principle S with the Lagrangian L in analogy to classical mechanics [11]

$$\delta S = \delta \int_{t_1}^{t_2} L(q_i, \dot{q}_i, t)\, \mathrm{d}t = 0\,, \tag{2}$$

where q_i and $\dot{q}_i$ are generalized coordinates and their time derivatives $\dot{q}_i = \partial q_i/\partial t$ characterizing the system, $i = 1, 2, \ldots, N$. The Lagrangian is chosen with the idea to find the extremal path between the starting and ending points in the variational integral S.

$$\frac{\partial L}{\partial q_i} - \frac{\mathrm{d}}{\mathrm{d}t}\frac{\partial L}{\partial \dot{q}_i} = 0\,. \tag{3}$$

In General Relativity, the Lagrangian describing the test particle motion is usually taken in the form $L = \mathrm{d}\tau/\mathrm{d}t$ [11]. It is obtained from the Schwarzschild metric, where $\mathrm{d}s = c\,\mathrm{d}\tau$ is the world line element, τ is the proper time, and t is the coordinate time. The metric in the quadratic form with the signature $[+,\ -,\ -,\ -]$ is given by

$$\mathrm{d}\tau^2 = (1 - 2\,r_g/r)\,\mathrm{d}t^2 - (1 - 2\,r_g/r)^{-1}\,\mathrm{d}r^2 - r^2\,\mathrm{d}\theta^2\,, \tag{4}$$

where the speed of light and the particle mass taken $c = 1$, $m = 1$.

The Lagrangian is

$$\begin{aligned} |L| &= \mathrm{d}\tau/\mathrm{d}t \\ &= \left((1 - 2\,r_g/r) - (1 - 2\,r_g/r)^{-1}(\mathrm{d}r/\mathrm{d}t)^2 - r^2\,(\mathrm{d}\theta/\mathrm{d}t)^2\right)^{1/2}\,, \end{aligned} \tag{5}$$

where $q_1 = r$ and $q_2 = \theta$.

Two constants of motion follow from the consideration of the ignorable temporal and angular variables. The conserved angular momentum is $l_0 = r\,(\mathrm{d}\theta/\mathrm{d}\tau)$. The conserved total energy comes out from the Hamiltonian

$$H = \sum_i \dot{q}_i \frac{\partial L}{\partial \dot{q}_i} - L\,, \tag{6}$$

that leads to (in a dimensionless form)

$$\epsilon_{rad} = (1 - 2\,r_g/r)\,\mathrm{d}t/\mathrm{d}\tau\,. \tag{7}$$

We put the subscript (rad) there because the expression does not contain l_0^2, hence, it must stand for the total energy in the particular case of pure radial motion when $l_0^2 = 0$. The corresponding equation of the radial motion is discussed later.

Finally, the expressions for the conserved total energy ϵ_0 for $l_0^2 \neq 0$ are found having the initial conditions fixed

$$\epsilon_0^2 = 1 - 2\,r_g/r + \beta_r^2 + l_0^2/r^2 - 2\,r_g\,l_0^2/r^3\,. \tag{8}$$

There $l_0^2/r^2 = \beta_\theta^2$ – the squared angular speed component. The term $\beta_r^2 = (\mathrm{d}r/\mathrm{d}\tau)^2$ is the squared radial speed component. The sum of two squared components makes the total squared speed of the test particle along an orbit, β^2, a function of radius.

Similarly to Classics, there must be two major types of a stable motion: bound motion for $\epsilon_0 < 1$ and unbound motion for $\epsilon_0 > 1$.

It should be noted that in literature, instead of Lagrangian, a useful concept of the GR effective potential concept V_{eff} is introduced in relationship with the Schwarzschild metric. In the quadratic-like form, it is

$$V_{eff}^2 = 1 - 2\,r_g/r + l_0^2/r^2 - 2\,l_0^2\,r_g/r^3 \tag{9}$$

related to the total energy ϵ_0

$$V_{eff}^2(r) = \epsilon_0^2 - \beta_r^2(r)\,. \tag{10}$$

It is used for approximate evaluations of GR Dynamics parameters [12, 13, 14].

2.4 The proper coordinate system with the proper time τ

As seen the Lagrangian solution, the GR equations of motion with non-zero angular momentum were derived from the quadratic metric form $\mathrm{d}\tau^2$, which is defined in the proper space-time (4). For this reason, the equations of motion are actually derived in terms of the proper coordinate time τ. Derivatives of the coordinates are correspondingly taken with respect to the time variable τ. This fact was acknowledged by Einstein and later by other GR researchers. The problem is that Astronomical observations are conducted in the so-called coordinate space-time with the coordinate time t, correspondingly. Consequently, the interpretation of the GR theoretical predictions is disputed, while

τ often is replaced with t for the comoving observer on the premises of weak-field conditions [7] (what is admitted in this work).

2.5 Formulation of the initial conditions, and physical treatment of the equations of motion

Let us set the initial conditions at the periapsis $r = r_0$: let it be $\theta_0 = 0$, the angular component of the velocity $\beta_\theta = \beta_0 \neq 0$, the radial speed component $\beta_r(r_0) = 0$, recall that the speed of light here is $c = 1$. The dimensionless parameter $\rho_0 = r_g/r_0$ characterizes the potential field strength. Next, we introduce a dimensionless variable, the inverted radius, $\xi = r_0/r$, $\xi_0 = 1$.

Now we have a set of desired equations, in which parameters are connected with the physical quantities determining the initial conditions $\rho_0 = r_g/r_0$, β_0^2. They are also related to the conserved total energy $\epsilon_0 = \epsilon(\xi)$ and other quantities, which are explicit functions of ξ: V_{eff}^2, β_r^2, β_θ^2, $\beta^2 = \beta_r^2 + \beta_\theta^2$. The conserved squared angular momentum is found in the form $l_0^2 = r_0^2\,\beta_0^2 = \beta_\theta^2/\xi^2$ (here $\beta_\theta = r\,\mathrm{d}r/\mathrm{d}\tau$). There are other useful equations

$$\begin{aligned} \epsilon_0^2 &= 1 - 2\,\rho_0 + \beta_0^2 - 2\,\rho_0\,\beta_0^2 \\ &= 1 - 2\,\rho_0\,\xi + \beta_0^2\,\xi^2 - 2\,\rho_0\,\beta_0^2\,\xi^3 + \beta_r^2(\xi)\,, \end{aligned} \tag{11}$$

and from this

$$\begin{aligned} \beta_r^2(\xi) &= \epsilon_0^2 - 1 + 2\,\rho_0\,\xi - \beta_0^2\,\xi^2 + 2\,\rho_0\,\beta_0^2\,\xi^3 \\ &= \beta_0^2 - 2\,\rho_0 - 2\,\rho_0\,\beta_0^2 + 2\,\rho_0\,\xi - \beta_0^2\,\xi^2 + 2\,\rho_0\,\beta_0^2\,\xi^3\,, \end{aligned} \tag{12}$$

$$\beta_\theta^2(\xi) = (r_0\beta_0)^2\,\xi^2\,, \tag{13}$$

$$\beta^2(\xi) = \beta_r^2(\xi) + \beta_\theta^2(\xi)\,, \tag{14}$$

$$V_{eff}^2(\xi) = \epsilon_0^2 - \beta_r^2(\xi)\,. \tag{15}$$

From the equality $\mathrm{d}\xi/\mathrm{d}\theta = \beta_r(\xi)/\beta_0$ easily proved, the equation of motion $\mathrm{d}\xi/\mathrm{d}\theta = f(\xi)$ follows:

$$\left(\frac{\mathrm{d}\xi}{\mathrm{d}\theta}\right)^2 = \left(1 - \frac{2\,\rho_0}{\beta_0^2} - 2\,\rho_0\right) + \frac{2\,\rho_0}{\beta_0^2}\,\xi - \xi^2 + 2\,\rho_0\,\xi^3\,. \tag{16}$$

A pair of two independent parameters determining a unique solutions could be ρ_0 and β_0^2 specified at the periapsis (or apoapsis),

or some their combination can be chosen, for example, ρ_0 and $\sigma_0 = \rho_0/\beta_0^2$. Obviously, there are three roots in the equation of motion but only any two of three are independent and determine the unique solution as well. Once an appropriate set of independent parameters is specified, the connection between any pair of them can be established.

3 The GR classification of orbits

3.1 Analytic connections between parameters of the motion equation and roots

The advantageous form of our presentation of the GR equation of motion (16) is that it is dimensionless and scaled to the initial condition $\xi_0 = 1$, and as such, it is governed by minimal two independent physical parameters fixed in the initial conditions. In the integral form, the exact unique solution to be computed is given by

$$\theta(\xi) = \int \frac{\mathrm{d}\xi}{\sqrt{\left(1 - \dfrac{2\,\rho_0}{\beta_0^2} - 2\,\rho_0\right) + \dfrac{2\,\rho_0}{\beta_0^2}\,\xi - \xi^2 + 2\,\rho_0\,\xi^3}}\,, \tag{17}$$

where integration is performed from the initial point $\xi = 1$ (which is one of the roots of the cubic polynomial presented under the radical) along the positive side of the cubic curve. Among three roots of the polynomial, any pair of them are physically independent It may have one or three real roots ξ_1, ξ_2, ξ_3.

In Einstein's problem, physical constraints are imposed on the equation, namely, conservations laws. Besides, in our approach, additional constraints come from the choice of the $\xi_0 = \xi_1 = 1$ in the initial conditions (variable rescaling). This allows us to easily determine other two roots without using Tartaglia and Cardano formulas for the roots of a cubic and then make a unique physical classification of solutions. Let

$$f(\xi) = 2\,\rho_0\,\xi^3 - \xi^2 + \frac{2\,\rho_0}{\beta_0^2}\,\xi + \left(1 - \frac{2\,\rho_0}{\beta_0^2} - 2\,\rho_0\right)\,, \tag{18}$$

then

$$\frac{f(\xi)}{\xi - 1} = 2\,\rho_0\,\xi^2 - (2\,\rho_0 - 1)\,\xi - \left(1 - \frac{2\,\rho_0}{\beta_0^2} - 2\,\rho_0\right) \tag{19}$$

is a quadratic polynomial in ξ with a simple expression for its roots:

$$\xi_{2,3} = \frac{1 - 2\,\rho_0 \pm \sqrt{1 + 4\,\rho_0 - 12\,\rho_0^2 - 16\,\rho_0^2/\beta_0^2}}{4\,\rho_0}\,. \tag{20}$$

3.2 Types of GR orbits in terms of roots

The Lagrangian problem formulation implies that all GR trajectories are periodic and time reversal, as in classical mechanic. However, while in classical mechanics the angular period is always $2\,\pi$, in GR the angular period takes larger values dependent on initial conditions. The GR perihelion advance effect is valid for any type of GR orbits including unbounded ones.

From the expression (11) for the total energy in the settings of the equation (16), it follows that a condition $\epsilon_0 \geqslant 1$ requires that $\beta_0^2 \geqslant 2\,\rho_0/(1 - 2\,\rho_0)$. Up to $\rho_0 \leqslant 1/4$, the trajectories corresponding to $\epsilon_0 \geqslant 1$ are all unbounded: either parabolic or hyperbolic. However, for $\rho_0 > 1/4$ and $2\,\rho_0/(1 - 2\,\rho_0) \leqslant \beta_0^2 < \rho_0/(1 - 3\,\rho_0)$, the total energy ϵ_0 is greater or equals to 1, but the trajectory of a particle is of a spiral fall type, i.e. the motion is bounded.

All possible variants of roots are shown in Figure 1. There are several cases when types of orbits depend, firstly, on the roots being real or complex, secondly, on specific values of ξ_2 and ξ_3. The integration of the equation (17) is performed from the first root $\xi_1 = 1$ over the positive part of $f(\xi)$ to the next root or up to the infinity, see example in Section 4.2. There are special points $\xi_2 = \xi_3$, $\xi_2 = 0$, $\xi_2 = 1$, and $\xi_3 = 1$, for which one needs to find the explicit relationships between ρ_0 and β_0^2 corresponding to three curves on (ρ_0, β_0^2) plane. These curves divide the plane of integration into four regions with a specific trajectory type. Six types of trajectories are possible: hyperbola, parabola, circle, over-circular precessing ellipse, sub-circular precessing ellipse, and spiral fall to the center, see Table 1 and Figure 2.

3.3 GR vs classical orbits

Einstein's equation of motion (16) is reduced to the corresponding classical one (in the contemporary form) if the cubic term is neglected. As discussed further, the same must be true for the GR equation of radial motion if the initial condition at $r = r_0$, $\beta_0^2 \neq 0$, $\beta_{r0} = 0$ in (16) is replaced with $\beta_0^2 = 0$, $\beta_{r0} \neq 0$, recall, the time variable τ in GR plays a role of the classical time t.

As we know, the classical orbits $r(\theta)$ are described by only one parameter $\sigma = r_0/\beta_0^2$ so that

$$\theta(\xi) = \int \frac{\mathrm{d}\xi}{(1-2\,\sigma) + 2\,\sigma\,\xi - \xi^2}\,, \tag{21}$$

using the same notations and initial conditions as in (16). The analytic solution is given by

$$r(\theta)/r_0 = (\sigma + (1-\sigma)\cos\theta)^{-1} \tag{22}$$

The σ presentation of classical theory is much more practically convenient than the conventional equations in terms of two geometrical parameters, – the eccentricity and the semilatus rectum, which are physically correlated, hence, not independent.

There are five types of classical orbits, solutions to the equation (22), examples of which are plotted in Figure 3.

The regions of the classical orbits in β_0^2 vs ρ_0 plane 4 are shown in Figure 4. While the first root is fixed, $\xi_1 = 1$, the second root is $\xi_2 = 2\,\sigma - 1$ (recall, $r = 1/\xi$). therefore, unbounded motion appears for ξ crossing zero value and going into negative side. The case, when $\xi_2 = 0$, that is when $\sigma = 1/2$, corresponds to a parabolic orbit. The case, when $\xi < 0$, that is when $\sigma < 1/2$, corresponds to a hyperbolic orbit. The other values of σ correspond to elliptic orbits. In particular, for $\sigma = 1$ one has $\xi_2 = 1$, which corresponds to a circular orbit. This picture can be compared with the analogous GR one in Figure 2.

Notice that types of orbits, which are similar in GR and classical mechanics, have different regions in $(\beta_0^2 - \rho_0)$ diagrams, this is also seen from a comparison of their parameters:

type of orbit	classical mechanics	general relativity
circular	$\beta_0^2 = \rho_0$	$\beta_0^2 = \dfrac{\rho_0}{(1-3\,\rho_0)}$, $\rho_0 \leqslant \frac{1}{4}$
parabolic	$\beta_0^2 = 2\,\rho_0$	$\beta_0^2 = \dfrac{2\,\rho_0}{(1-2\,\rho_0)}$, $\rho_0 < \frac{1}{2}$

It is also seen that in GR a new type exists, which we call a spiral fall, see Figure 5. This type of orbits does not exists in classical mechanics. It is characterized a particle fall on the center under specific conditions. In literature, it is associated with strong fields in the Black Hole environments.

4 Analytic and Numerical Solutions

4.1 Elliptic function method

The equation (17) can be recognized as an elliptic integral of the first kind (see any textbook on elliptic functions and elliptic integrals, for example, [15, 16]). It can be solved by means of the Weierstrass elliptic function $\wp$ [15, §20.6].

The $\wp$-function satisfies the following differential equation

$$(\wp'(z))^2 = 4\,(\wp(z))^3 - g_2\,\wp(z) - g_3\,, \tag{23}$$

where parameters g_2 and g_3 are known as the elliptic invariants. Conversely, given the equation

$$\left(\frac{\partial u}{\partial z}\right)^2 = 4\,u^3 - g_2\,u - g_3\,, \tag{24}$$

One gets the general solution

$$u = \wp(\pm z + \alpha)\,, \tag{25}$$

where α is the constant of integration. The equation $y^2 = 4\,x^3 - g_2\,x - g_3$ is known as the Weierstrass normal form of an elliptic curve. Therefore, the equation (16) can be solved in terms of the Weierstrass elliptic function $\wp$. Moreover, the solution can be given in a convenient form $r(\theta)$.

This approach is well known, the following are just a few related articles that employed the Weierstrass elliptic function: Hagihara suggested classification of the trajectories in a gravitational field of Schwarzschild [4], Kraniotis and Whitehouse studied the perihelion precession of the orbit of the planet Mercury around the Sun [6], Lämmerzahl discussed the experimental basis of General Relativity [17].

In order to determine the corresponding parameters for $\wp$-function and the expression for the solution of (16), it is necessary to transform our equation into Weierstrass normal form. There are several ways to do this.

Consider the following linear substitution

$$\xi = \frac{2}{\rho_0}\,x + \frac{1}{6\,\rho_0}\,. \tag{26}$$

The equation (16) becomes

$$\left(\frac{\partial x}{\partial \theta}\right)^2 = 4x^3 - \left(\frac{1}{12} - \frac{\rho_0^2}{\beta_0^2}\right) x - \left(\frac{1}{216} - \frac{1+3\beta_0^2}{12\,\beta_0^2}\,\rho_0^2 + \frac{1+\beta_0^2}{2\,\beta_0^2}\,\rho_0^3\right), \tag{27}$$

that is

$$\begin{aligned} g_2 &= \frac{1}{12} - \frac{\rho_0^2}{\beta_0^2}\,, \\ g_3 &= \frac{1}{216} - \frac{1+3\,\beta_0^2}{12\,\beta_0^2}\,\rho_0^2 + \frac{1+\beta_0^2}{2\,\beta_0^2}\,\rho_0^3\,. \end{aligned} \tag{28}$$

Therefore,

$$r(\theta) = \frac{6\,\rho_0\,r_0}{12\,\wp(\theta+\alpha; g_2, g_3) + 1}\,. \tag{29}$$

From the theory of Complex Analysis, it follows that the function $\wp$ is a meromorphic function in the complex plane. It is doubly periodic with two linearly independent periods $2\,\omega_1$ and $2\,\omega_2$. When the roots of the cubic $4\,x^3 - g_2 x - g_3$ are all real, one of the periods is purely imaginary, and another is real. The real period corresponds to the angular period of motion described by the equation (16).

The function $\wp$ is a complex-valued function, however along the line $\alpha + \theta$, where orbital angle θ varies, the imaginary part of it vanishes. The value $\wp(\alpha) = (6\,\rho_0 - 1)/12$ corresponds to the initial condition $(r = r_0, \theta = 0)$ and equals to one of the roots of the cubic polynomial (27). This is the property of the function $\wp$ that values $\wp(\omega_1)$, $\wp(\omega_2)$ and $\wp(-\omega_1 - \omega_2)$ are all three roots of the cubic. Therefore, the value of α is either ω_1, or ω_2, or $-\omega_1 - \omega_2$.

Algorithms for computing the periods for the case of real coefficients may be found in literature, see, for example, [18, Algorithm 7.4.8] or [19, §3.7]. The use the real arithmetic–geometric mean allow one to compute both values rapidly with a high degree of precision. The theory of this method is described in [20]. It has been generalized in [21] allowing for complex-valued coefficients.

In practice, the software packages produce the corresponding $\wp$-function and compute the periods without requiring a user to transform the equation into the Weierstrass form. Most major mathematical software systems support computation with elliptic functions. We have chosen to use SAGE [22] because it is freely available, highly flexible and very efficient. Calculations can be performed

with arbitrary precession, we used precision of 600 significant digits here. Moreover, the computations can be performed on-line at `http://cloud.sagemath.com` without requiring a user to install software on a personal computer. SAGE also provides access to numerous other open source scientific packages, in particular, we used PARI/GP [23].

4.2 Numerical integration

Recall the integral form of the GR equation of motion (17). As in the above analytical solution, there are several singular cases where the integral does not converge. Depending on values of two parameters ρ_0 and β_0, the integration (17) is performed from $\xi_1 = 1$ to either ξ_2 or ξ_3.

Numerical integration procedure in PARI/GP can take into account the asymptotic behavior of integrating function at end points and compute the result with chosen arbitrary precision. Our numerical solution are in complete agreement with the solution produced using Weierstrass $\wp$-function.

As an example, consider a case when the cubic has three roots, e.g. $\rho_0 = 0.05$, $\beta_0 = 0.04$. Then, the cubic polynomial in the equation (17) becomes

$$f(\xi) = 0.1\,\xi^3 - \xi^2 + 2.5\,\xi - 1.6\,, \tag{30}$$

with three roots $\xi_1 = 1$, $\xi_2 \approx 2.44$ and $\xi_3 \approx 6.56$, see Figure 6. The initial condition dictates the starting point $r_0 = 1/\xi = 1$, $\theta_0 = 0$, the integration (17) is performed from $\xi = 1$ to $\xi = \xi_2$:

$$\theta(\xi) = \int_1^{\xi_2} \frac{\mathrm{d}\xi}{\sqrt{0.1\,\xi^3 - \xi^2 + 2.5\,\xi - 1.6}}\,. \tag{31}$$

The full integral from 1 to ξ_2 corresponds to the periapsis position $r_p = 1/\xi_2 \approx 0.41$, $\theta_p = \int_1^{\xi_2} 1/\sqrt{f(x)}\,\mathrm{d}\xi \approx 4.53$, which is the closest approach to the central mass. From this point, the test particle motion continues in counter-clock direction. At the apoapsis point $r_a = r_0 = 1$, $\theta_a = 2\,\theta_p \approx 9.07$, the particle completes the first period, see Figure 7.

4.3 Time dependent exact solution

The time dependent problem in both Newtonian and GR mechanics can be solved only by numerical integration. In GR, the equation of

motion, for example, follows from 12, where $\beta_r(\xi) = \mathrm{d}r/\mathrm{d}\tau$. Therefore,

$$\tau(\xi) = -\int \frac{\mathrm{d}\xi}{\beta_0\,\xi^2\sqrt{\left(1-\dfrac{2\,\rho_0}{\beta_0^2}-2\,\rho_0\right)+\dfrac{2\,\rho_0}{\beta_0^2}\,\xi-\xi^2+2\,\rho_0\,\xi^3}}\,. \quad (32)$$

The expression under the radical is exactly the same as in (17), and integration is performed along the same ξ interval. The expression (32) corresponds to the elliptic integral of the third type. In contrast to the case of the elliptic integral of the first type, there is no analytical expression similar to (29). Nevertheless, the theory of Complex Analysis implies that the solution $r(\tau)$ exists, and it is periodic. For practical purpose, we compute the integral (32) numerically.

5 Final results: Mercury's orbit

5.1 Input data

For our calculations we used the most recent input data taken from [24, 25, 26], namely:

- the speed of light $c = 299792458$ m/s;
- the Solar mass parameter (heliocentric gravitational constant) $\mu = 1.32712440041 \times 10^{20}$ m^3/s^2, that makes Schwarzschild radius $r_{sch} = 2953.2500770$ m;
- Mercury's perihelion distance $r_p = 4.600 \times 10^{10}$ m;
- Mercury's aphelion distance $r_a = 6.982 \times 10^{10}$ m;

From these data, we have $\rho_0 = 3.21 \times 10^{-8}$. The second parameter $\beta_0^2 = 3.87 \times 10^{-8}$ can be obtained from r_p, r_a and ρ_0. The value β_0^2 has been rounded to three significant figures for fixing identical initial conditions in both classical and GR computations. This makes Mercury's velocity at perihelion $v_p = 5.898 \times 10^4$ m/s, which agrees with [26]. The aphelion value (up to three decimal figures) then becomes $r_a = 6.9811764705882 \times 10^{10}$ meters in classical theory, and 14237.080 meters shorter in GR.

5.2 The computation

The equation (16) is numerically specified (from here and below we print up to eight significant digits while the calculations were per-

formed with 600 digits):

$$\left(\frac{\mathrm{d}\xi}{\mathrm{d}\theta}\right)^2 = 6.42\times10^{-8}\,\xi^3 - \xi^2 + 1.6589147\,\xi - 0.65891479\,. \qquad (33)$$

The first two roots, the inverse values of r_p and r_a are rescaled: $\xi_1 = 1$ corresponding to the perihelion, $\xi_2 = 0.65891486$ corresponding to the aphelion, and the third root is $\xi_3 = 1.5576322\times10^7$. The corresponding Weierstrass form (27) of the above equation is

$$\left(\frac{\mathrm{d}x}{\mathrm{d}\theta}\right)^2 = 4\,x^3 - 0.083333307\,x - 0.0046296274 \qquad (34)$$

with roots $x_1 = -0.083333317$, $x_2 = -0.083333323$, $x_3 = 0.16666664$. However, in SAGE and in PARI/GP we do not need to transform the equation into Weierstrass form in order to compute the periods. The software allows for arbitrary cubic polynomial with scaled major coefficient, produces the corresponding $\wp$ elliptic function and computes the semi-periods. For our input the half periods are $\omega_1 = 3.141592904530036$ and $\omega_2 = 20.40947598338886\,i$. Direct numerical integration reproduces the same result for the orbital half period ω_1 up to 300 significant digits. Taking into account Mercury's sidereal orbit period 0.2408467 Earth years, we obtain the known value of the Mercury's perihelion advance ≈ 42.98 arcsec per century.

5.3 Comparison with classical mechanics

The question arises how to compare the Mercury's output data, including results of time dependent problem $r(\tau)$, with the analogous classical data, when the GR effect is very small. The relative difference between the GR angular half period and the classical value of π is 7.99×10^{-8}. This number alone will actually ignore an analysis of time-dependent solutions.

The comparison problem is that the predictions depend on formulation of initial conditions in two theories and the criterion of comparison. Ideally, Astronomers conduct observations of object's motion in time, during which the 3D-coordinate system must be fixed in space, so that a varying distance from the Sun $r(t)$ is measured in time with the orbital angle varying in time as well $\theta(t)$. They want theoreticians to give them a chart of the object's trajectories $r(\theta(t))$ predicted by

both theories with a common set of initial data, including physical parameters variable for best fitting. In practice, the situation is severely aggravated by interactions of planets no considered here.

We denote for simplicity the time variable t in both theories assuming the commonly accepted argument that the GR proper time τ in the Mercury's orbital motion can be replaced with the coordinate time t due to weak-filed conditions. As noted above, we assume the ideal picture of a single test particle orbiting about the Sun, mass of which is concentrated in the origin of the coordinate system.

The following ideal initial conditions are fixed for both theories: at $t = 0$, the test particle is positioned at $\theta = 0$, at the minimal distance (perihelion) from the Sun r_p, with a maximal orbital speed of the particle β_0. We suggest *the three events scheme* of the comparison, including time-dependent analysis, explained below.

Results of comparison in the ideal conditions are presented in Table 2, Table 3, Table 4. The three events are specified in terms of orbital characteristics predicted by both theories at three distinct time moments. Namely,

- Event 1: t_1 when $\theta_{cl} = \pi$ (classical half-period)
- Event 2: t_2 when $\theta_{gr} = \pi$ (gr half-period is not reached yet)
- Event 3: t_3 when $\theta_{gr} = \pi + \Delta\theta$ (gr half-period), $\Delta\theta$ the GR angular advance)

At each event, all orbital characteristics predicted by both theories are compared in details. Particularly, it is seen that "the GR particle" compared to "the classical particle", moves on average faster, its aphelion is smaller, consequently, its angular period is advanced, while the temporal period is smaller (about 1 seconds per period). Those differences of the $10^{-7} - 10^{-8}$ order or less are very small and require special technique for their exact computations.

From the above results, one can draw two important conclusions.

First, dynamics of GR observable effect cannot be physically understood just having the angular advance prediction $\Delta\theta$. Indeed, it must be observable in a set of physical characteristics varying in time. The requirement of precise timing of orbital revolution is crucial for assessments of the GR effects with respect for corresponding classical values. In our chart, it is assumed that the running of time is observable exactly, that is, ideal standard atomic clocks and other ideal measuring tools are used in a rigidly fixed coordinate system.

Second, the differences to be observed are practically very small, as seen from the example of the GR Mercury's temporal period being only one seconds shorter than in classical theory. This makes the criterion of verifiable GR predictions and treatments of observations a challenging methodological problem. Clearly, the ideal initial conditions we fixed, is a special part of the practical problem. In particular, the precisions of the input data needs to be proved essentially better than the GR effect. For example, r_p and β_0 should be known, at least, at the 10^{-9} level. Notice, the reality of data precision requirements is out of the scope of this work.

We think that the GR Mercury' problem should be reconsidered in view of our findings. The suggested methodology of the space-time chart for comparison of different theories of gravitational dynamics can be also applied in other Astronomical and Cosmological challenging problems of matter motion.

6 Final results: Black Hole environment

6.1 Orbital motion

The equation (16) is used, since it is valid for all ranges of field strength. Therefore, for the first time, we used it for obtaining the exact solutions for strong field conditions. For simplicity, we assume, as in literature, that the central gravitational attractor is a point-like body. Recall, the time variable in the GR equations of motion with non-zero angular momentum is the proper time τ, but it is often replaced with the coordinate time t interpreted as a comoving time.

The GR particle orbital motion in strong gravitational fields, say, $\rho_0 < 1/4$, are associated with the Black Hole environment. The concept of Black Hole used in Astrophysics suggests that a material object of mass greater than several solar masses, undergoes the hypothetical process of gravitational collapse, thus, the assumption of a point source in this case is not a mathematical abstraction but a physical phenomenon. The equation (16) is actually valid for any central, not necessary point-like, mass. The wonderful property of the equation is that it the same in the whole range of field strength, say, in case of planetary motion and motion of bodies in the Black Hole vicinity. The types of possible trajectories, of course, depends on the conditions.

As an example of orbital motion, consider the field strength $\rho_0 = 0.05$, and $\beta_0^2 = 0.04$. As seen from tables of orbit classification, it is of sub-circle type with notably precessing orbit, see in Figure 7. The angular half period there is about 4.53 radians, which is by 44% larger than the corresponding classical value π, the time period is by 7% smaller, the periapsis by 38% smaller, and the velocity at periapsis by 63% higher. The only possible type of Black Hole orbits for $\rho_0 > 1/4$ is of spiral fall, as seen from tables of orbit classification. The example of spiral fall orbit is shown in Figure 5.

The equation implies the conservation laws and periodic time-reversal solutions. One can be surprised to find out that these properties are preserved in spiral fall orbits. As the parameter $\beta_0^2 \to 0$, the orbital precession frequency and the particle speed rapidly increase and the motion never approaches the radial fall.

6.2 Free radial fall

As previously noted, GR Dynamic equations of orbital motion are reduced to classical ones when the GR cubic term of interference of angular momentum with the potential energy is neglected. Because the angular momentum in the particle free radial fall is zero by definition, the GR equation of the radial motion has to be automatically coincide with the corresponding classical one.

In conventional GR Dynamics, however, the radial fall equation differs from the classical one. The reason for that is that the GR equation is derived with the use of GR expression of conserved total energy ϵ_{rad} (7) [12], also [14, 27]. Below, we follow the conventional derivation of equations starting from the initial conditions in the expression for ϵ_{rad}:

$$\epsilon_{rad} = (1 - 2\,r_g/r)\,\mathrm{d}t/\mathrm{d}\tau = (1 - 2\,r_g/r_{ic})\,\mathrm{d}t_{ic}/\mathrm{d}\tau_{ic}\,. \qquad (35)$$

Assume the initial conditions are fixed at "far away". To avoid the infinite time of motion from infinity, let us introduce the "far-away" distance r_{fa} however great but finite, and let the initial inward speed be $(\mathrm{d}r/\mathrm{d}t)_{fa} = (1 - 1/\gamma_{fa}^2)^{-1/2}$. Then, the inward speed of a particle in the radial fall is found:

$$(\mathrm{d}r/\mathrm{d}t)_{fa}(r) = (1 - 2r_g/r)\left(1 - (1 - 2r_g/r)/\gamma_{fa}^2)\right)^{1/2}\,. \qquad (36)$$

Here, $\gamma_{fa} = E_0/m_0 \geq 1$ is considered the "far-away" total energy. Respectively, the formula is interpreted in terms of the "far-away"

observer whose wristwatch shows the coordinate time t. At the same time, let us introduce the so-called "shell observer" placed at some point $r_{shell} < r_{fa}$, which is not fixed in the initial conditions, whose wristwatch must show the proper time τ_{shell}. Then, the radial speed $\mathrm{d}r_{shell}/\mathrm{d}\tau_{shell}$, viewed by the "shell" observer in accordance with (35), must be given by

$$(\mathrm{d}r/\mathrm{d}\tau)_{shell}(r) = \left(1 - (1 - 2r_g/r)/\gamma_{fa}^2\right)^{1/2} . \qquad (37)$$

The formula (36) has to be understood from the viewpoint of "far-away" observer. It shows that the particle sent from infinity to the center begins to accelerate, but at some point, it starts decelerating. The motion looks "strange", however. The matter is that the particle, before approaching the Schwarzschild radius $r_{sch} = 2r_g$, at some point dependent on γ_{fa}, starts decelerating: the higher initial kinetic energy, the farther the deceleration point from the center. For $\gamma_{fa} \geq \sqrt{3/2}$, the particle will never accelerate in a gravitational field. The gravitational force exerted on the particle becomes repulsive in the entire space.

Quite differently, the formula (37) shows that, from the viewpoint of "shell" observer, the particle always accelerates. When crossing the Schwarzschild sphere, it reaches the speed of light. In the internal space, the particle is considered not observable (due to "light trap"), likely, its motion becomes superluminal till it "crashes" at the center. This picture is widely known in association with the particle radial fall onto Black Hall.

Let us compare the above GR predictions with classical theory. The formula (37), as well as the GR equations of orbital motion, describe a particle motion in terms of time variable τ. In both cases, the descriptions look similarly to that in classical theory, in which the time variable is, of course t. It would be naturally expected that the time variable in the above GR cases might be also the coordinate time t. Contrarily, in (36), having no classical analogy, it might be τ. Why it did not happened, is seen from the form of the Schwarzschild metric $\mathrm{d}\tau^2$, from which the GR Dynamics equations are derived. The metric is originally defined in the proper space-time yielding the proper time as a dynamic variable, and so the GR equations of motion. As for "the strange" GR decelerating motion with the variable t, it does not look physically possible.

The readers could put a number of questions concerning a strict theoretical justification of the above GR radial equations. Having

no clear understanding of their derivations, we would join them in addressing the questions, in particular, the τ vs t issue, to the authors of referred works and other experts in the field.

6.3 Schwarzschild radius and particle velocity

In classical mechanics, the test particle having a small angular momentum always follows an elliptical orbit of the sub-circular type. Its periapsis can be however close to the center, while the particle crosses the Schwarzschild sphere at the speed of light and can move further faster than the speed of light. Classical superluminal motion takes place in the radial fall as well.

As we learned, there is a similarity of classical and GR theories in description of elliptic and radial motions (GR equations with the proper time variable are meant). In both theories, the particle can cross the Schwarzschild sphere and can move faster than light. However, interpretations of superluminal motion are different. Classical description of motion in the strong field is considered invalid since the theory is not relativistic. Quite opposite, it is valid in GR, however, according to the general opinion and in agreement with the SR theory, the observable superluminal motion does not exists in physical reality. "The far-away observer" does not detect the superluminal motion by his wristwatch, while "the comoving observer" does not "feel" the event of crossing the Schwarzschild sphere [14].

There is another difference. In GR, there is a class of the spiral fall motion, what cannot be in the classical theory, see Table 1. In the sub-circle motion, it behaves differently, namely, a periapsis distance corresponds to the maximal value of $\xi_2 > 1$, i.e. for $\rho_0 < 1/6$ and $16\,\rho_0/(1+4\,\rho_0-12\,\rho_0^2) \leqslant \beta_0^2 < \rho_0/(1-3\,\rho_0)$, see Table 1, Figure 2. It cannot reach a position $\xi_2 \geqslant 1/(2\,\rho_0)$. It is seen, the particle can cross the Schwarzschild sphere only in the type of spiral fall motion, in some close inner and outer regions as well. The particle speed can be easily calculated.

From the conservation laws, we obtain the expression for the total speed of the particle along the trajectory:

$$\beta^2(\xi) = \beta_0^2 - 2\,\rho_0 - 2\,\rho_0\,\beta_0^2 + 2\,\rho_0\,\xi + 2\,\rho_0\,\beta_0^2\,\xi^3\,. \qquad (38)$$

From this, the total speed at Schwarzschild radius is

$$\begin{aligned} v^2(r_{sch}) &= 1 - 2\,\rho_0 + \beta_0^2 \left(1 - 2\,\rho_0 + \frac{1}{4\,\rho_0^2}\right) \\ &= (1 - 2\,\rho_0)\left(1 + \beta_0^2\right) + \frac{\beta_0^2}{4\,\rho_0^2}\,. \end{aligned} \tag{39}$$

Depending on the initial velocity, the full speed at Schwarzschild radius can be smaller than, equals to or greater than the speed of light. Figure 8 shows the condition on ρ_0 and β_0^2 in order to achieve the speed of light at Schwarzschild radius.

There is some ambiguity in GR vs classical theory comparison because the GR Dynamics operates with two types of time variable: both τ and t in the pure radial motion, and only τ in the orbital motion. The interpretation depends on the field strength. This issue is discussed in [14] in view of Einstein's methodology of space-time curvature as a manifestation of gravity.

7 Conclusions

This work is intended to encourage researchers in Astronomy and Astrophysics to study planetary and galaxy dynamics in view of our new results concerning the use of classical and relativistic gravitational theories and their interpretation of non classical effects in the whole range of field strength. The questions are raised concerning unambiguous physical formulations of exact versus approximate solutions to be further discussed. The author will appreciate any critical comments and questions related to the results.

8 References

[1] Albert Einstein. Erklärung der Perihelbewegung des Merkur aus der allgemeinen Relativitätstheorie. Sitzungsberichte der Königlich Preussischen Akademie der Wissenschaften zu Berlin, 1915. See also "The Collected Papers of Albert Einstein". vol. 6, Princeton University Press, (1996).

[2] Kirill Vankov. The Problem of Particle Motion in the Schwarzschild Field: Critical Methodological Analysis, Exact Numerical Solution, and the Alternative. *The General Science Journal*, 2016.

[3] Kirill Vankov. General Relativity Mercury's Anomaly Prediction: What and How to Test? *The General Science Journal*, 2016.

[4] Yusuke Hagihara. Theory of the relativistic trajectories in a gravitational field of Schwarzschild. *Annales de l'Observatoire astronomique de Tokyo*, 31:67–176, 1931.

[5] Subrahmanyan Chandrasekhar. *The mathematical theory of black holes*, volume 69 of *International Series of Monographs on Physics*. Clarendon Press/Oxford University Press, New York/Oxford, 1983.

[6] Georgios Kraniotis and Steve Whitehouse. Compact calculation of the perihelion precession of Mercury in general relativity, the cosmological constant and Jacobi's inversion problem. *Classical and Quantum Gravity*, 20(22):4817, 2003.

[7] Anatoli Vankov. General Relativity Problem of Mercury's Perihelion Advance Revisited. arXiv:1008.1811 [physics.gen-ph], 2010.

[8] Yvonne Choquet-Bruhat. *General relativity and the Einstein equations*. Oxford University Press, 2009.

[9] Karl Schwarzschild. On the Gravitational Field of a Mass Point According to Einstein's Theory. *General Relativity and Gravitation*, 35(5):951–959, 2003. Über das Gravitationsfeld eines Massenpunktes nach der Einsteinschen Theorie. Sitzungsberichte der Königlich Preussischen Akademie der Wissenschaften zu Berlin, Phys.-Math. Klasse 1916, 189–196.

[10] Peter Gabriel Bergmann. *Introduction to the Theory of Relativity*. Kessinger Publishing, 2008.

[11] Vladimir Fock. *The Theory of Space, Time and Gravitation*. Pergamon, 1959.

[12] Charles W. Misner, Kip S. Thorne, and John Archibald Wheeler. *Gravitation*. W. H. Freeman and Co, San Francisco, 1973.

[13] Robert Wald. *General Relativity*. University of Chicago Press, 1984.

[14] Edwin F Taylor, John Archibald Wheeler, and Edmund William Bertschinger. *Exploring Black Holes: Introduction to General Relativity*. Addison-Wesley, 2010.

[15] Edmund Taylor Whittaker and George Neville Watson. *A course of modern analysis*. Cambridge university press, 1927.

[16] Richard Courant and Adolf Hurwitz. *Funktionentheorie*. Verlag von Julius Springer, Berlin, 1929.

[17] Claus Lämmerzahl. Testing Basic Laws of Gravitation–Are Our Postulates on Dynamics and Gravitation Supported by Experimental Evidence? In *Mass and Motion in General Relativity*, pages 25–65. Springer, 2011.

[18] Henri Cohen. *A course in computational algebraic number theory*, volume 138 of *Graduate Texts in Mathematics*. Springer, 1993.

[19] John Cremona. *Algorithms for modular elliptic curves*. Cambridge University Press, 1997.

[20] Jean-Benoît Bost and Jean-François Mestre. Moyenne arithmético-géométrique et périodes des courbes de genre 1 et 2. *Gaz. Math*, 38:36–64, 1988.

[21] John Cremona and Thotsaphon Thongjunthug. The complex AGM, periods of elliptic curves over C and complex elliptic logarithms. *Journal of Number Theory*, 133(8):2813–2841, 2013.

[22] W. A. Stein et al. *Sage Mathematics Software (Version 6.4)*. The Sage Development Team, 2014. `http://www.sagemath.org`.

[23] The PARI Group, Bordeaux. *PARI/GP version* `2.7.1`, 2014. available from `http://pari.math.u-bordeaux.fr/`.

[24] K.A. Olive and Particle Data Group. Review of Particle Physics. *Chinese Physics C*, 38(9):090001, 2014.

[25] U.S.NAVY. The Astronomical Almanac. Constants., 2017. Avaialable at `http://asa.usno.navy.mil/SecK/Constants.html`.

[26] NASA. Lunar and planetary science. Mercury fact sheet., 2016. See `http://nssdc.gsfc.nasa.gov/planetary/factsheet/mercuryfact.html`, accessed on 2017-08-03.

[27] S. I. Blinnikov, L. B. Okun, and M. I. Vysotskii. Critical velocities $c/\sqrt{3}$ and $c/\sqrt{2}$ in the general theory of relativity. *Physics-Uspekhi*, 46(10):1099–1103, 2003.

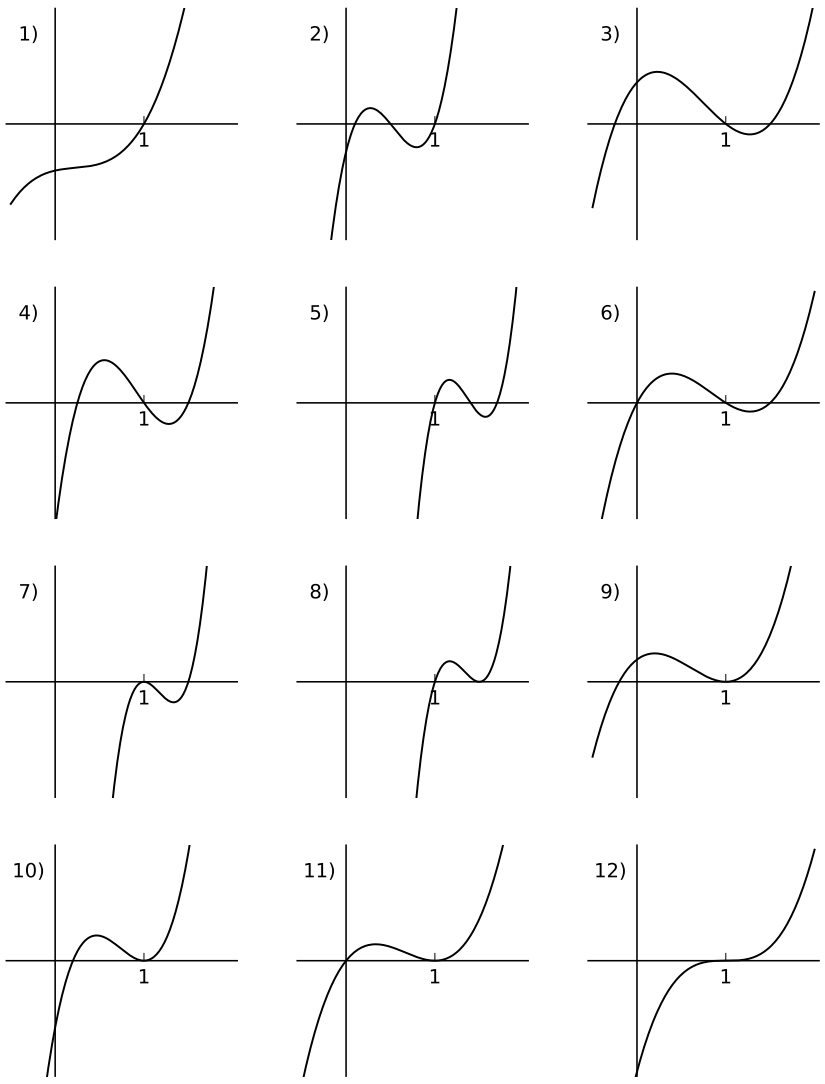

Figure 1: All possible roots of a cubic r.h.s. of (16):
1) complex ξ_2, ξ_3 roots; 2) $\xi_3 \leqslant \xi_2 < 1$; 3) $\xi_2 < 0$, $\xi_3 > 1$;
4) $0 < \xi_2 < 1$, $\xi_3 > 1$; 5) $1 < \xi_2 < \xi_3$; 6) $\xi_2 = 0$, $\xi_3 > 1$;
7) $\xi_2 = 1$, $\xi_3 > 1$; 8) $1 < \xi_2 = \xi_3$; 9) $\xi_2 < 0$, $\xi_3 = 1$;
10) $0 < \xi_2 < 1$, $\xi_3 = 1$; 11) $\xi_2 = 0$, $\xi_3 = 1$; 12) $\xi_2 = 1$, $\xi_3 = 1$.

Table 1: Orbits classification: SF – spiral fall, H – hyperbola, P – parabola, C – circle, OC – over-circle, SC – sub-circle.

condition on ξ_2, ξ_3	relation between β_0^2 and ρ_0	orbit type	Fig. 1 ref.
ξ_2, ξ_3 not real or $\xi_3 < 1$	$\rho_0 < \frac{1}{6}\,, \quad \beta_0^2 < \frac{16\,\rho_0^2}{1+4\,\rho_0-12\,\rho_0^2}$ or $\frac{1}{6} < \rho_0 < \frac{1}{3}\,, \quad \beta_0^2 < \frac{\rho_0}{1-3\rho_0}$ or $\rho_0 \geqslant \frac{1}{3}$	SF	1), 2)
$\xi_2 < 0$, $\xi_3 > 1$	$\rho_0 \leqslant \frac{1}{4}\,, \quad \beta_0^2 > \frac{2\rho_0}{1-2\rho_0}$ or $\frac{1}{4} < \rho_0 < \frac{1}{3}\,, \quad \beta_0^2 > \frac{\rho_0}{1-3\rho_0}$	H	3)
$\xi_2 < 1 < \xi_3$	$\rho_0 < \frac{1}{4}\,, \quad \frac{\rho_0}{1-3\,\rho_0} < \beta_0^2 < \frac{2\rho_0}{1-2\rho_0}$	OC	4)
$1 < \xi_2 < \xi_3$	$\rho_0 < \frac{1}{6}\,, \quad \frac{16\,\rho_0^2}{1+4\,\rho_0-12\,\rho_0^2} < \beta_0^2 < \frac{\rho_0}{1-3\rho_0}$	SC	5)
$\xi_2 = 0$, $\xi_3 > 1$	$\rho_0 < \frac{1}{4}\,, \quad \frac{2\rho_0}{1-2\rho_0}$	P	6)
$\xi_2 = 1$, $\xi_3 > 1$	$\rho_0 < \frac{1}{6}\,, \quad \beta_0^2 = \frac{\rho_0}{1-3\,\rho_0}$	C	7)
$1 < \xi_2 = \xi_3$	$\rho_0 < \frac{1}{6}\,, \quad \beta_0^2 = \frac{16\,\rho_0^2}{1+4\,\rho_0-12\,\rho_0^2}$	SC, SF	8)
$\xi_2 < 0$, $\xi_3 = 1$	$\frac{1}{4} < \rho_0 < \frac{1}{3}\,, \quad \beta_0^2 = \frac{\rho_0}{1-3\,\rho_0}$	H, C, SF	9)
$0 < \xi_2 < 1 = \xi_3$	$\frac{1}{6} < \rho_0 < \frac{1}{4}\,, \quad \beta_0^2 = \frac{\rho_0}{1-3\,\rho_0}$	OC, C, SF	10)
$\xi_2 = 0$, $\xi_3 = 1$	$\rho_0 = \frac{1}{4}\,, \quad \beta_0^2 = 1$	P, C, SF	11)
$\xi_2 = \xi_3 = 1$	$\rho_0 = \frac{1}{6}\,, \quad \beta_0^2 = \frac{1}{3}$	C, SF	12)

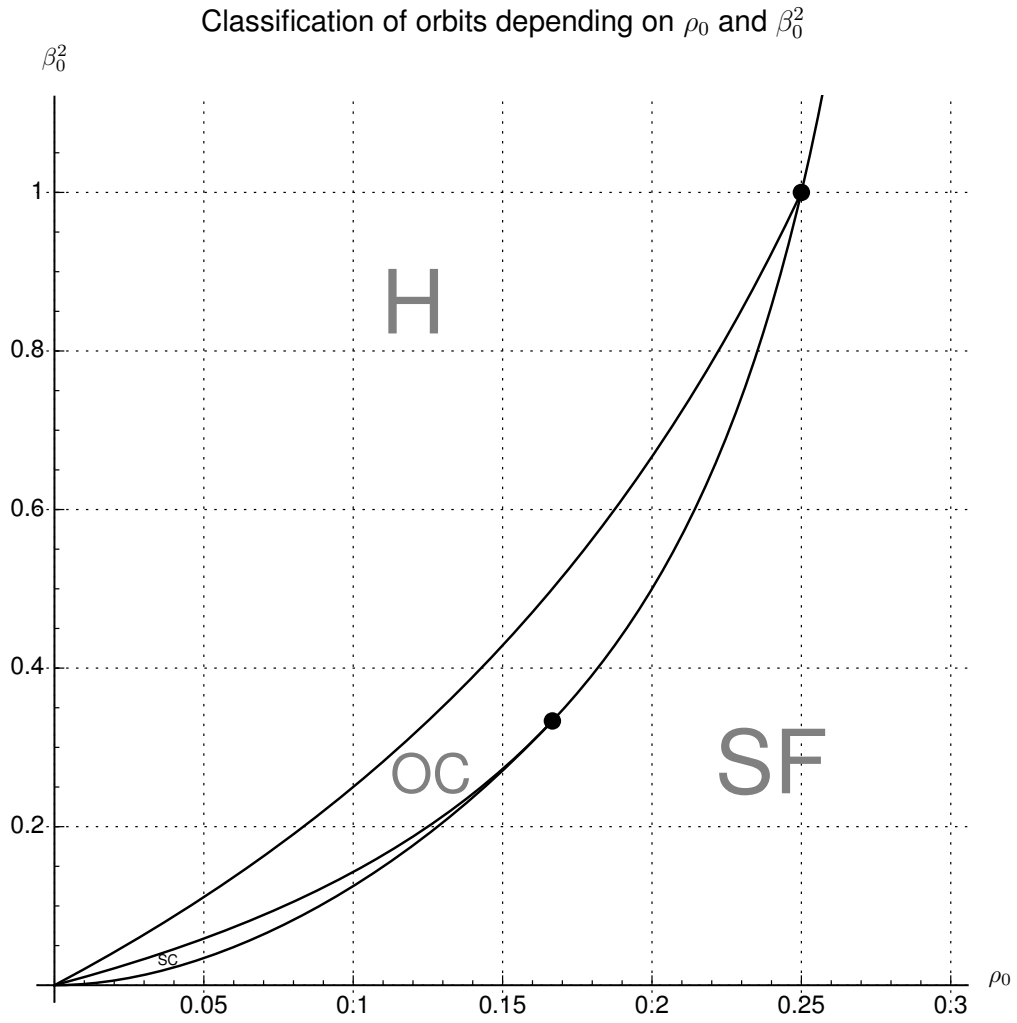

Figure 2: GR orbit classification on (ρ_0,β_0^2) plane: H – hyperbolic type; OC – over-circular type; SC – sub-circular type; SF – spiral fall type; parabolic type – line next to H; circular orbits – middle curve from 0 till $\rho_0 = 1/6$ continuing to $\rho_0 = 1/4$.

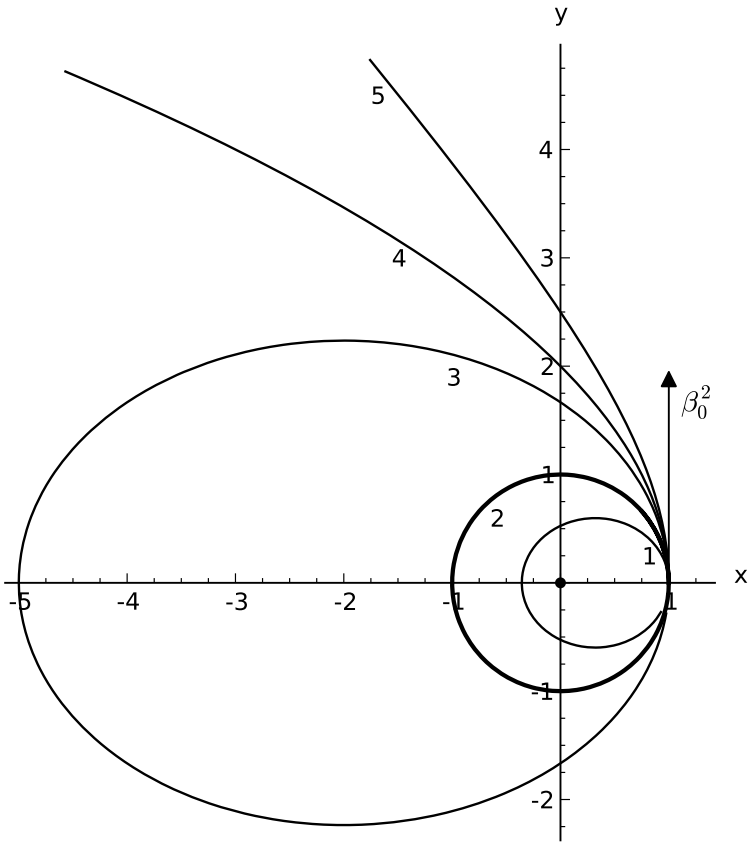

Figure 3: All possible orbits in Classical Mechanics: 1 – sub-circle, 2 – circle, 3 – over-circle, 4 – parabola, 5 – hyperbola.

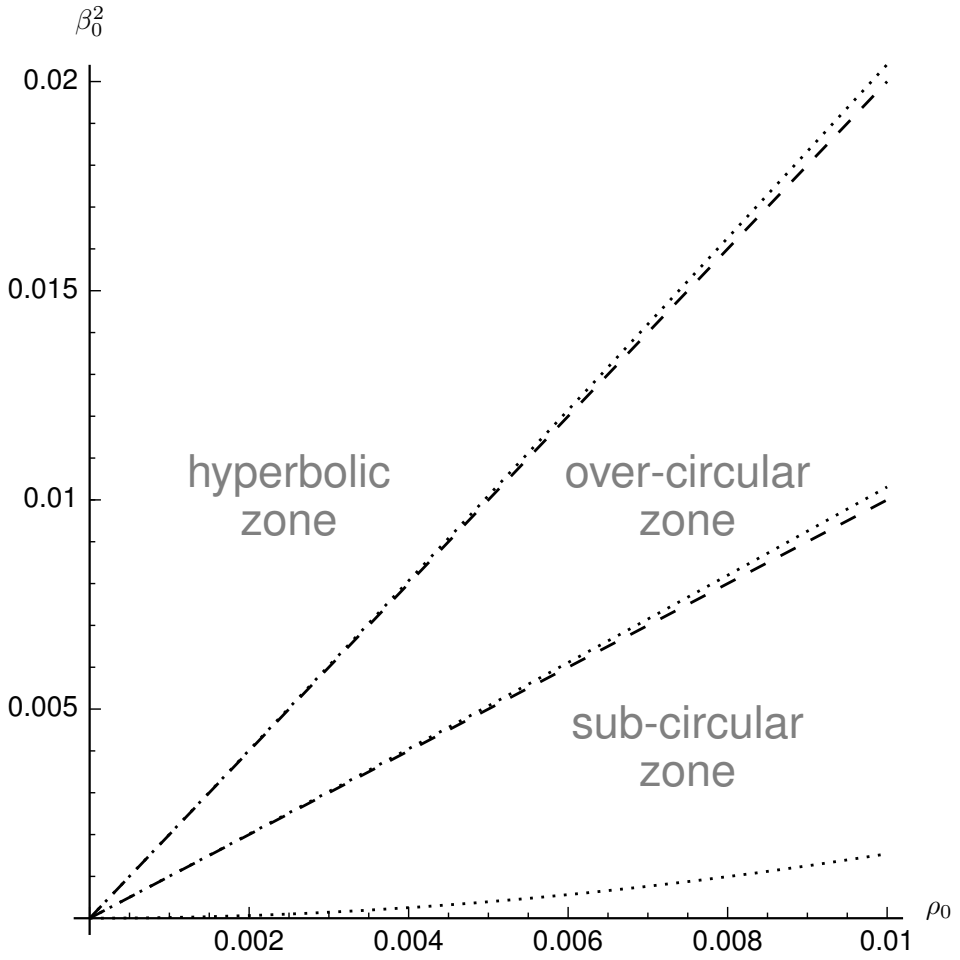

Figure 4: Orbit classification in classical mechanics (dashed lines): the top region corresponds to hyperbolic orbits, the top dashed line – parabolic orbits, in between the dashed lines – over-circular orbits, the bottom dashed line – circular orbits, below – sub-circular orbits. In GR theory (dotted curves) there is an additional (at the very bottom, below the dotted line) region with spiral-fall type of orbits. When ρ_0 and β_0^2 are small, the orbit classification in classical mechanics becomes similar to that in GR.

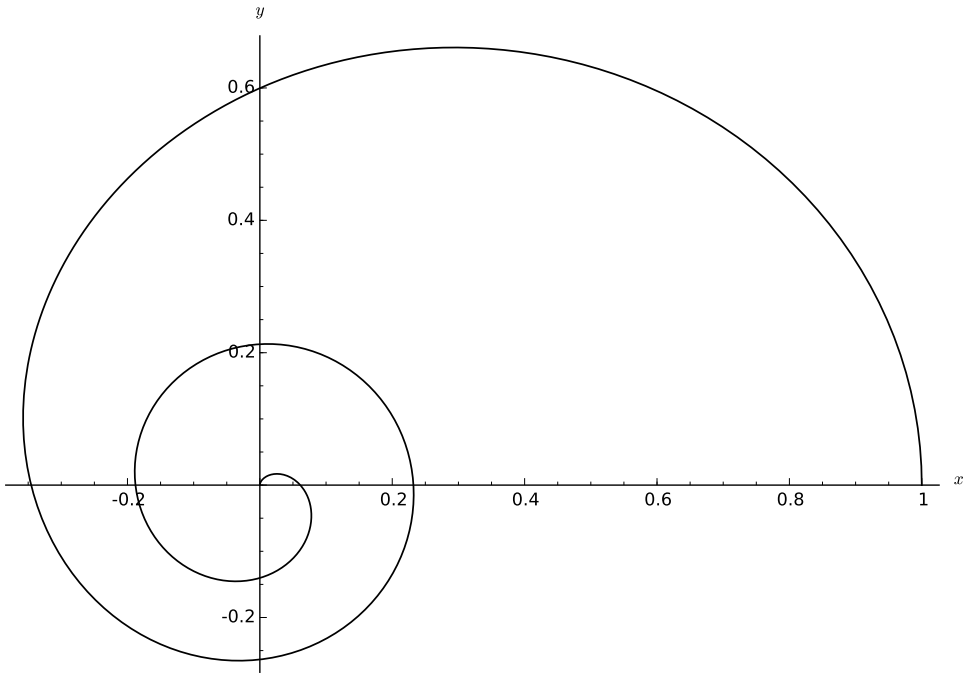

Figure 5: Spiral fall trajectory for $\rho_0 = 0.05$, $\beta_0^2 = 0.03$. Shown only half period.

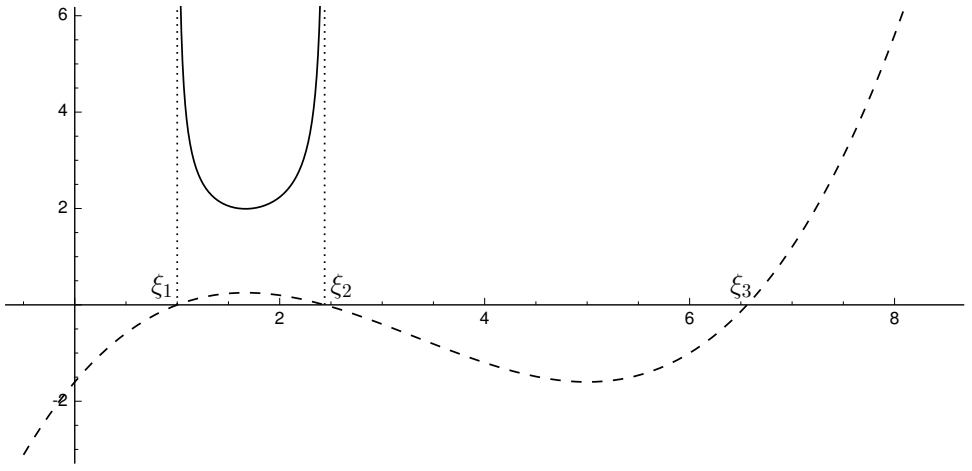

Figure 6: Typical case of polynomial $f(\xi)$ with three roots (here $\rho_0 = 0.05$, $\beta_0 = 0.04$, the dashed line). The integration is performed from $\xi_1 = 1$ to ξ_2 under the solid line.

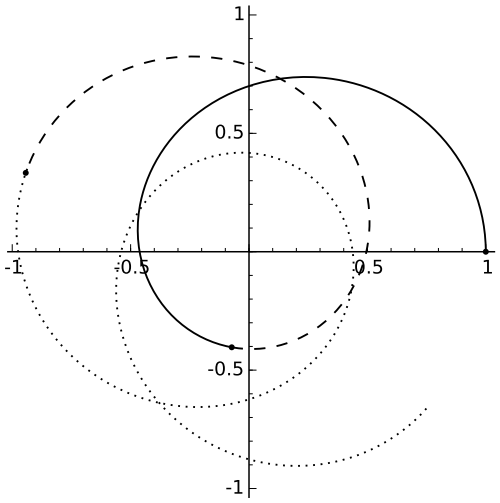

Figure 7: Orbit for $\rho_0 = 0.05$ and $\beta_0 = 0.04$. Starting point (1,0), following solid line first periapsis at point (0.41,4.53), following dashed line first period completed at point (1,9.07), continuing by dotted line for another period. All points are given in polar coordinates.

Input parameters:			
dimensionless $\rho_0 = r_g/c^2$	3.21×10^{-8}		
dimensionless β_0^2	3.87×10^{-8}		
dimensionless r_0	1		
Scaling quantities:			
the speed of light c	299792458 m/s		
$\mu_0 = r_g c^2$	$1.32712440041\times10^{20}$ m^3/s^2		
perihelion r_p	4.6×10^{10} m		
velocity at perihelion	58976 m/s		
Output:			
Computed characteristics	classical theory	GR - Classics	relative
angular period (radians)	$2\,\pi$	5.019×10^{-7}	7.988×10^{-8}
time full period T (s)	7599967.916 s	-1.111 s	-1.461×10^{-7}
aphelion r_a (m)	69811764705.882 m	-14237.080 m	-2.039×10^{-7}
velocity at aphelion (m/s)	38860.233 (m/s)	7.924×10^{-3} (m/s)	2.039×10^{-7}
full period orbit length (m)	1.800×10^{11} m	-6301.537 m	-3.501×10^{-8}
squared total energy ϵ^2	0.9999999744999999995	-2.485×10^{-15}	-2.485×10^{-15}

Table 2: Comparison of GR vs classical mechanics results for Mercury. We fixed perihelion and velocity at perihelion as well as the gravitational field strength to be the same for GR and classical theory.

Event 1: $\vec{r}_{gr}$ at π position			
time elapsed from $t = 0$	3799982.952 s		
$\lvert\vec{\Delta}r\rvert$	41611.534 m		
GR	**Classical theory**	**GR - Classics**	**relative**
(distance to the Sun) r_1	69811764705.880 m	-14237.078 m	-2.039×10^{-7}
$\Delta\theta$	3.141592094 rad	5.601×10^{-7} rad	1.783×10^{-7}
(trajectory length) Δs	179978534889.556 m	15280.087 m	8.490×10^{-8}
Event 2: GR at aphelion			
time elapsed from $t = 0$	3799983.402 s		
$\lvert\vec{\Delta}r\rvert$	41611.541 m		
	Classical theory	**GR - Classics**	**relative**
(distance to the Sun) r_2	69811764705.881 m	-14237.079 m	-2.039×10^{-7}
$\Delta\theta$	3.141592344 rad	5.601×10^{-7} rad	1.783×10^{-7}
(trajectory length) Δs	179978552408.130 m	15280.090 m	8.490×10^{-8}
Event 3: Classics at aphelion (at π position)			
time elapsed from $t = 0$	3799983.958 s		
$\lvert\vec{\Delta}r\rvert$	41626.836 m		
	Classical theory	**GR - Classics**	**relative**
(distance to the Sun) r_3	69811764705.882 m	-14237.081 m	-2.039×10^{-7}
$\Delta\theta$	π rad	5.601×10^{-7} rad	1.783×10^{-7}
(trajectory length) Δs	179978573989.757 m	15280.095 m	8.490×10^{-8}

Table 3: Three events comparison: Event 1. t_1^{cl} when $\theta_{cl} = \pi$ (classical half-period); Event 2. t_2^{gr} when $\theta_{gr} = \pi$ (gr half-period is not reached yet); Event 3. t_3^{gr} when $\theta_{gr} = \pi + \Delta\theta$ (gr half-period). The quantity $|\Delta r| = |\vec{r}_{gr} - \vec{r}_{cl}|$ is the absolute difference of the radius vectors GR with respect to classical theory at the indicated event. The same meaning have other quantities $\Delta q = q_{gr} - q_{cl}$.

	Classical theory	**GR**
Difference between "Event 2" and "Event 1" (time 0.451 s)		
$\Delta\theta$	2.509×10^{-7} rad	2.509×10^{-7} rad
$\Delta r(t)$	1.971×10^{-3} m	5.689×10^{-4} m
Δs	17518.574 m	17518.578 m
Difference between "Event 3" and "Event 1" (time 1.006 s)		
$\Delta\theta$	5.601×10^{-7} rad	5.601×10^{-7} rad
$\Delta r(t)$	2.834×10^{-3} m	-2.945×10^{-4} m
	39100.201 m	39100.209 m
Difference between "Event 3" and "Event 2" (time 0.555 s)		
Δs	3.091×10^{-7} rad	3.091×10^{-7} rad
$\Delta r(t)$	8.634×10^{-4} m	-8.634×10^{-4} m
Δs	21581.627 m	21581.631 m

Table 4: Absolute differences of main orbital characteristics in GR and classical theories at the events $(2-1)$, $(3-1)$, $(3-2)$.

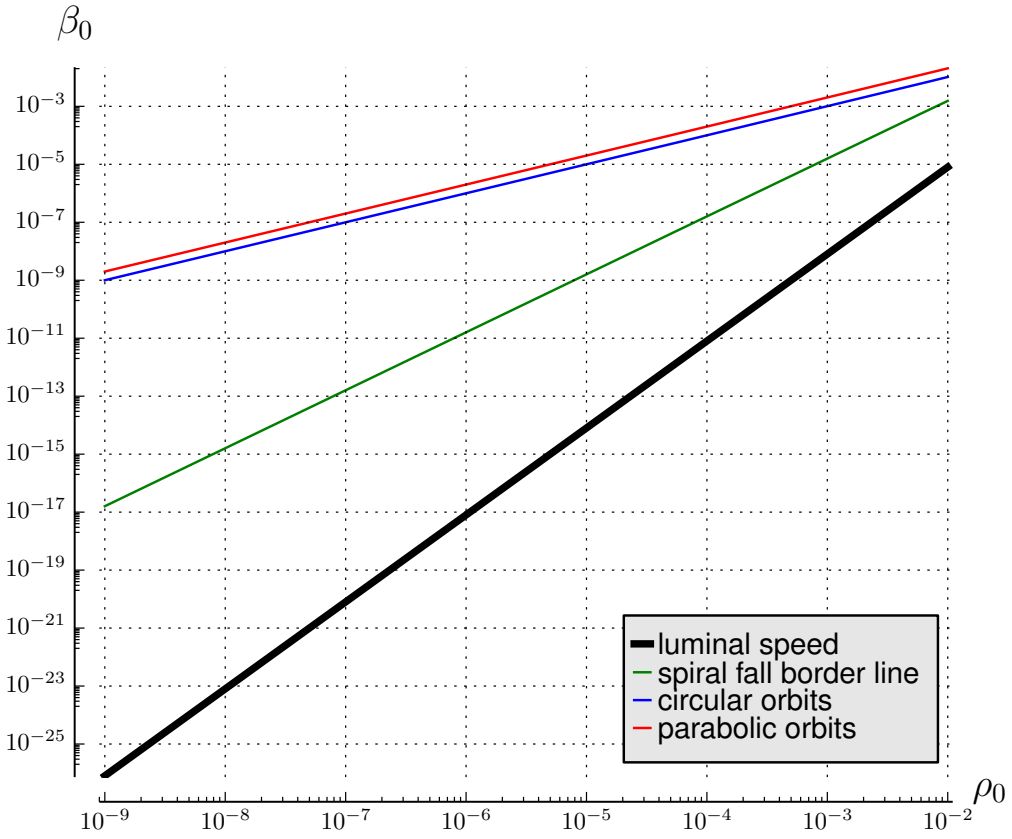

Figure 8: Conditions for achieving luminal speed at Schwarzschild radius. For the values (ρ_0, β_0^2) below the black line the full speed of a particle at Schwarzschild radius is lower than the speed of light, between the black and the green lines, the speed is greater than the speed of light.